

HIGH IMPEDANCE FAULTS DIAGNOSIS IN POWER DISTRIBUTION SYSTEM BASED ON ADALINE HARMONIC ANALYSIS

M. Jannati¹, R. Keivani¹ and L. Eslami¹

¹ Department of Electrical Engineering, Saveh Branch, Islamic Azad University, Saveh, Iran.

Corresponding Author Email: Mohsen.Jannati@aut.ac.ir

ABSTRACT: In a power distribution system, physical contact between the phase conductors and their surrounding objects such as trees and buildings is a probable incident. Known as High Impedance Fault (HIF), this situation may lead to fatal ignition or electric shock caused by the arcing. Although short circuit situations can be recognized by the usual relays in power distribution systems, HIF incidents cannot be detected easily by the common protection equipment. Since HIF increases the load current very slightly, it may be misdiagnosed as a usual overload. Therefore, HIF detection is a challenging issue in power distribution systems. The first step to overcome this problem is finding an appropriate model for the HIF arcing. In this paper, different types of HIF models are studied and then a complete model along with its simulation method is provided. Afterwards, an ADALINE-based algorithm for HIF detection in power distribution networks is proposed which uses a new harmonic criterion. Unlike the various solutions already presented for HIF detecting, the proposed approach is very simple and its online implementation is not problematic. Furthermore, a typical distribution network in the presence of Distributed Generation (DG) resources is simulated through the EMTPWorks environment. Simulation results verify the accuracy and the quickness of the proposed approach.

Keywords: Fault Detection; High Impedance Fault; ADALINE; Distribution Systems.

1. INTRODUCTION

Since the amplitude of the current resulted from the HIF is below the detection threshold limit of traditional protection relays, the existing protections are not able to detect it [1]. On the other hand, Failure in the HIF detection threatens the public safety. In this situation actually an energized conductor is released in the fault location which can hurt the people seriously or cause fire burning [2-3].

Initial investigations on HIF detection were based on the settings of existing relays like over-current relays and earth relays. However, these approaches reduced the performance of relays and made unnecessary interruptions in the system servicing. In further research, it was suggested to produce a new relay which recognizes the contact of the current-carrying conductor with the human body. But some other investigations revealed that different human bodies show different behaviors in the face of electrical shocks. Therefore, most the detection approaches concentrated on detecting the fault before the happening of this fatal contact with the conductors. In recent years various techniques for HIF detection have been introduced. A comprehensive category of these techniques is given in [4].

In [5], the comparative changes in magnitude and phase of the third harmonic were introduced as a criterion for HIF detection. In [6], HIF detection was fulfilled by using the third and third and a half harmonic components of the fault current. The main idea of the approach presented in [7] is related to the asymmetric waveform of HIF current. They also used this fact that the distortion of the current waveform in the switching activity happens in a shorter time period than in the HIF occurrence. In [8] three parameters of odd harmonics frequencies, even harmonics frequencies and interstitial harmonics frequencies were utilized for detecting the HIF. The method proposed in [9] was based on the current waveform components extracted by Prony technique. In fact, this method monitors the current waveform and recognizes the HIF in the case of finding descending DC values in the signal. A new approach based on the neutral voltage alterations and zero-order currents was introduced in [10].

This technique contains two independent algorithms called "neutral voltage analysis" and "residual current analysis". However, the practical implementation of this approach needs integrating the SCADA post with the modern relays. The authors of [11] used decision tree method along with the random forest model to recognize HIFs which do not accompany any arc happening. Others [12], state space model, optimization and analytical methods were employed to solve the HIF detection issue. A new approach utilizing the Support Vector Machine (SVM) was proposed [13]. Elsewhere [14], a new solution based on the statistical pattern recognition was suggested. In this method desired characteristics are extracted from one cycle of the current crossing the distribution feeder by use of TT transform which is a kind of time-time transformation. Utilizing Wavelet Transform with improved capability for index extraction was suggested in [15]. Others [16] show the HIF detection issue was tackled by applying the energy of frequency intervals and the multi-layer Perceptron Neural Network. In [17], Multi-Decomposition Analysis of discrete wavelet transform was employed to extract the indexes of distorted waveforms caused by HIF. The authors in [18] utilized digital signal processing which employs a new application of discrete wavelet Multi-resolution Signal Decomposition method to extract the indexes of distorted waveforms. In [19], researchers used a tool based on Mathematical Morphology (MM) which can be utilized as a module along with the traditional over-current relays.

The remainder of the paper is organized as follows: First, an overview on HIF arc modeling approaches is given in Section 2. In Section 3 a comprehensive HIF arcing model is developed and its basic structure is studied. The typical distribution network is introduced in Section 4. In Section 5 HIF voltage and current characteristic is described. Structure of ADALINE is presented in Section 6. Section 7 describes the proposed algorithm for HIF diagnosis. Section 8 deals with the obtained simulation results. Conclusion and references are presented in Section 9.

2. HIF MODELS

In 1985 the first model for HIF was proposed by connecting a resistance to the system at the fault location [20]. Considering the experiments performed by Emanuel in 1990, a model for HIF was proposed based on the sparks nature when the conductor comes into contact with the ground [21]. This model has been formed from two DC power supplies and two diodes paralleled each other inversely. Likewise, a resistance and a reactance control the amplitude and current of the fault. This model has been shown in Figure 1.

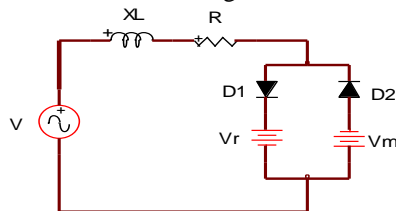


Figure 1. Emanuel model for HIF.

In 1993, this resistance and the reactance were replaced by two nonlinear resistances (according to Figure 2) to consider the nonlinear behavior of the ground in some way [22].

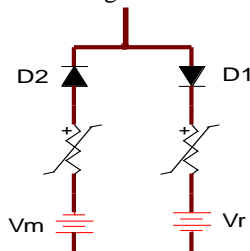


Figure 2. HIF model presented in 1993.

A model formed of nonlinear impedance, time variable voltage power supplies and TACS (Transient Analysis of Control System) control switches was introduced in 1996 [23].

A HIF model by using two series nonlinear resistance shown in Figure 3 was presented in 2001. One of the resistances models the nonlinearity and asymmetry of the fault current and another shows the transient in time of fault occurrence [24].

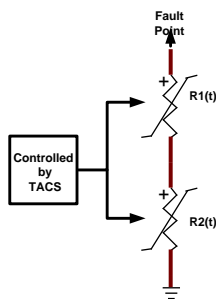


Figure 3. HIF model by using two nonlinear resistances.

In 2003, for producing HIF current the model in Figure 4 was used in which R_p and R_n model fault resistances. Also for modeling the asymmetry of current, resistances were selected different [25].

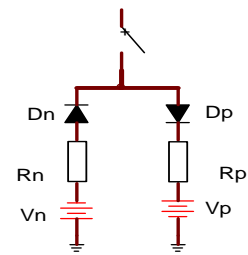


Figure 4. HIF model presented in 2003.

HIF model of Figure 5 including a nonlinear resistance, two diodes and two DC sources with amplitudes which change in every half cycle randomly has been presented in 2004. Average changing and variance of the DC voltage source amplitude were determined related to the type of the earth surface [26].

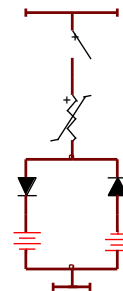


Figure 5. HIF model by using nonlinear resistance and Changing DC sources.

In 2005, another HIF model illustrated in Figure 6 was introduced. In this model linear resistance $R(t)$ is the ground equivalent resistance, $r(t)$ is the arc dynamic state, and DC and AC sources model the asymmetry of fault current and quenching alterations of arcs respectively [27].

A nonlinear resistance controlled by EMTP models was introduced as an arc model in 2006 [28].

In 2007 a HIF model was presented by N. Elkalashy *et al* [29], which is more precise and more complete compared with the other available ones. However, the arc behavior in two positive and negative half cycles has been considered the same in the simulations of this model for simplicity. In this paper, a completely precise model simulated through EMTPWorks is presented. The modeling procedure is described step-by-step. It is evident that precise modeling leads to more precise simulation results and extracting a more comprehensive solution.

In order to achieve the characteristic of a HIF happening in a 20 kV distribution network, an experiment has been conducted [29]. The experiment contains determining the resistance of a tree and attaining the characteristic of HIF fault. The experiment circuit and the process description have been addressed [29].

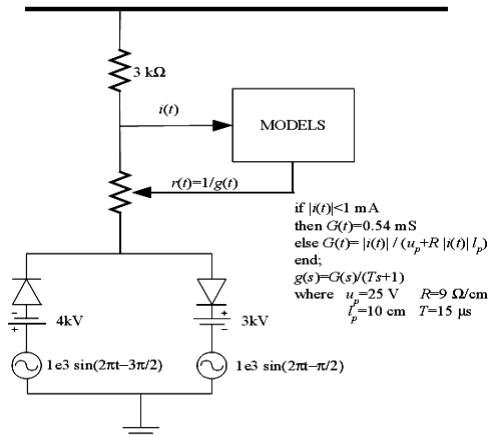


Figure 6. HIF model presented in 2005 [27].

3. DYNAMIC MODEL OF HIF ARC

The fault voltage and current related to two different locations including leaves and branch of a tree have been shown in Figure 7. If the fault is resulted from a contact between the conductor and the foliage, the arc is suddenly quenched once the fault current crosses the zero point. When the fault voltage increases in fault point, the arc is established again. Figure 7.a shows the magnified diagram of this phenomenon.

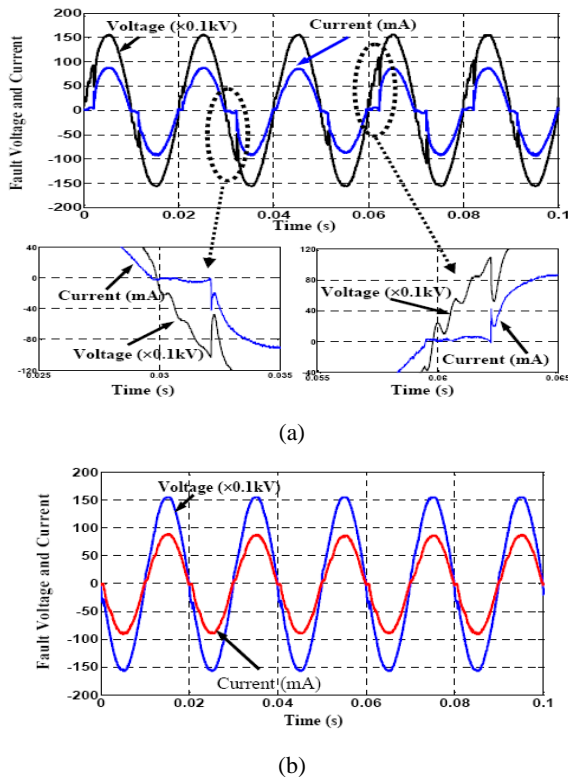


Figure 7. Voltage and current waveforms when (a) fault happens in foliage (b) fault happens in the branches [29].

Figure 8 shows the voltage-current characteristic of tested HIF current for Figure 7.a. As seen, the behavior of HIF arc is different in two positive and negative half cycles. The arc model proposed in this paper considers this difference in voltage- current characteristic between two half cycles.

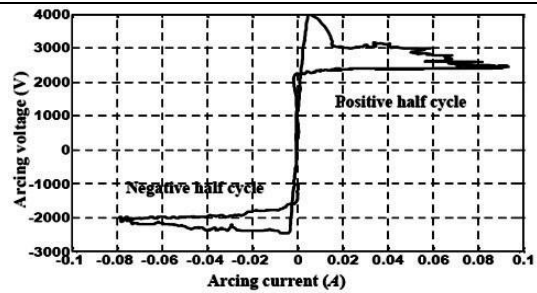


Figure 8. Experimental voltage-current characteristic of HIF arc [29].

The first complete model describing the arc behavior has been presented in [29]. Equation (1) is a thermal-based equation which is used to determine the changeable arc conductance in this model:

$$\frac{dg}{dt} = \frac{1}{\tau} (G - g) \tag{1}$$

where, g is the time variable conductance of arc, $G = |i| / V_{arc}$ is the stationary arc conductance, $|i|$ is the absolute value of the arcing current, V_{arc} is the arcing voltage constant value and τ is the arc time constant. All the above parameters are determined in a way that the results match the practical results.

To calculate these parameters, the characteristic shown in Figure 8 is utilized. Moreover, equation (2) is used to calculate the value of τ :

$$\tau = Ae^{Bg} \tag{2}$$

where A, B are constants and similar to V_{arc} have different values in two positive and negative half cycles of fault voltage and current and are estimated by the experimental results. The values related to the positive half cycle are:

$V_{arc} = 2520V, A = 6.6E - 5$ and $B = 41977$ in [29]. For the negative half cycle the values are:

$V_{arc} = 2100V, A = 2.0E - 5$ and $B = 85970.30$. Indeed all these values are calculated for Figure 7.a.

General dynamic model of the arc denoted in Figure 9, has been shown in Figure 10. A network similar to the test circuit shown in Figure 9 is employed to simulate this experiment in EMTWorks. The arc dynamic model shown in this circuit is derived from the above equations. In addition, input values of this circuit are used to obtain the waveforms of Figure 7.a.

The CTR control signal used for controlling the integrator has been presented in [30]. Indeed, this part of model depicts the arc sudden quenching in zero crossing moment. The controllable integrator output is calculated by integrating the main input until the control signal is high. Once the control signal turns to low, the integrator output will be the RES signal. Actually, RES signal gives the arc resistance at quenching moment. Based on the experimental results, resistance value is a time variable function. During the first 1ms interval after the arc quenching, it has a slope of $0.5 M\Omega/ms$ and after that 1 msec interval its slope turns to $4M\Omega/ms$. Thus, the sudden quenching and reigniting of arc can be simulated using the CTR signal achieved by the

results of Figure 7.a [30].

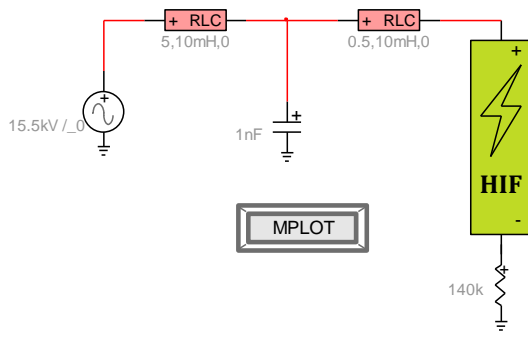


Figure 9. Network used for HIF modeling in EMTWorks.

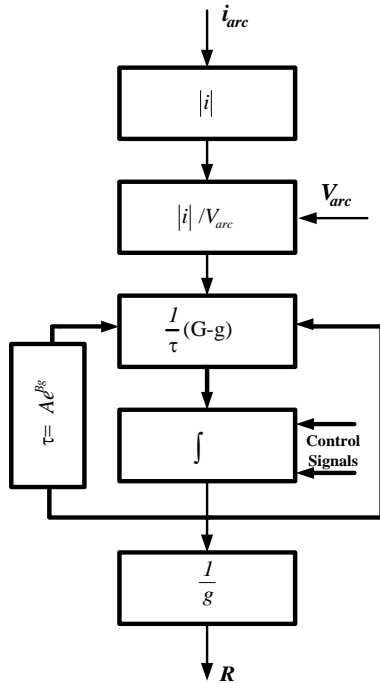


Figure 10. HIF arc complete model.

4. UNDER-STUDY DISTRIBUTION SYSTEM

In order to test the proposed approach, the distribution system presented in [30] is developed according to the CIGRE models used for integrating the distributed generation in medium voltage distribution networks. As illustrated in Fig. 11, the distribution system is composed of 4 generation nodes with different distributed generation technologies, 2 load nodes and a node connected to a 20 kV distribution network. A 1000 kW doubly fed induction generator wind turbine (DFIG WT), two 1200 kW permanent magnet wind turbines connected to the grid through the full converters (FC WT), and a solar-photovoltaic (PV) installation of 1000 kW of rated power form the distribution network in which the generation nodes are located. The loads are placed at nodes 3 and 7 with a nominal power of 1800+ j 0.87 kVA and 5200+j0.87 kVA, respectively. The electrical parameters of the distribution

network are as follows:

Operation voltage $V_{GI}= 20 \text{ kV}$

Thevenin impedance $Z_{thGI}=40.84 \Omega$

The connection between nodes is done by transmission.

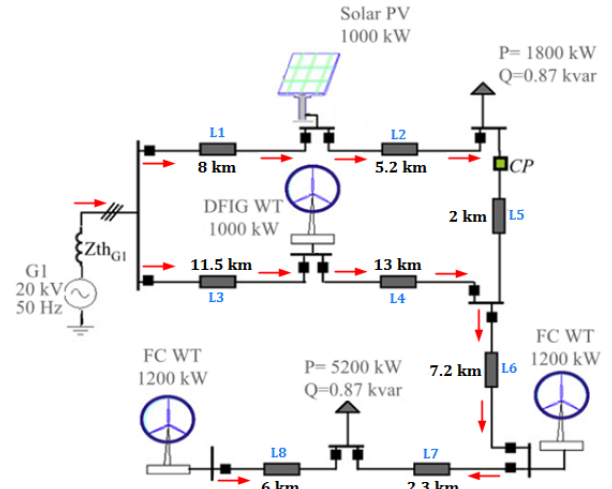


Figure 11. Under-study distribution system.

5. HIF VOLTAGE AND CURRENT CHARACTERISTIC

In order to extract an appropriate algorithm for HIF detecting, it is necessary to have a complete understanding about the HIF behavior. For this purpose and according to the explanation provided in Section 3, a HIF is applied in 4km line L1 of the test network given in Section 4. Fig. 12 shows the voltage and current waveforms at the location where HIF happens. The fault occurs at 40 msec. The voltage waveform has not changed appreciably before and after the HIF occurrence, but the current waveform has been considerably changed. The periodic changes of the current waveform happen at zero crossing points when the HIF arc repeatedly turns on and off. Hence, the current waveform can be used for HIF detecting. However, the problem is that the current waveform is not available at the beginning of the line where the measuring devices are placed. Fig. 13 illustrates the voltage and current waveforms of the faulty phase at the beginning of the line. It is obvious that HIF cannot be detected by use of this waveform. Therefore, in this study the residual current is utilized instead of the faulty phase current. The residual current at each moment is obtained by adding the currents of three phases:

$$i_{res}(t) = i_a(t) + i_b(t) + i_c(t) \tag{3}$$

where $i_{res}(t)$ indicates the residual current at each moment t . Fig. 13 shows the waveform of the residual current for the HIF discussed before at the beginning of the line. According to the figure, the behavior of the residual current waveform is very similar to that of the HIF current at the fault location. Thus, HIFs can be easily recognized by extracting the harmonics of the residual current signal and creating a harmonic index. In order to extract the harmonics of the residual current signal at the least possible time, ADALINE is applied to this study.

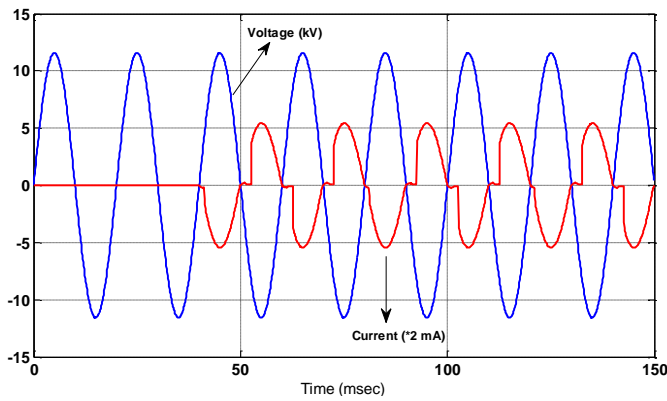


Figure 12. Voltage and current waveforms at HIF location.

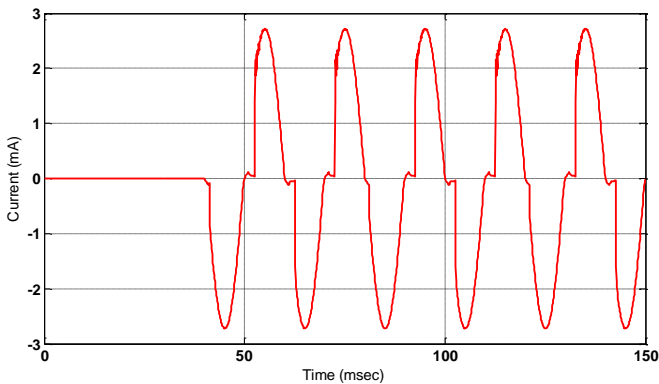


Figure 13. The residual current waveform at the beginning of the line when HIF occurs.

6. STRUCTURE OF ADALINE

Known as an artificial neural network, ADALINE has two layers with n inputs and one output. ADALINE output is a linear combination of its inputs [31]. ADALINE has some specific main characteristics including its easy online training according to the inputs and the changes of the target response, the ability of being applied to the learning weights, and its simple structure which contributes to its easy implementation on the hardware. The structure of an ADALINE has been shown in Fig. 14.

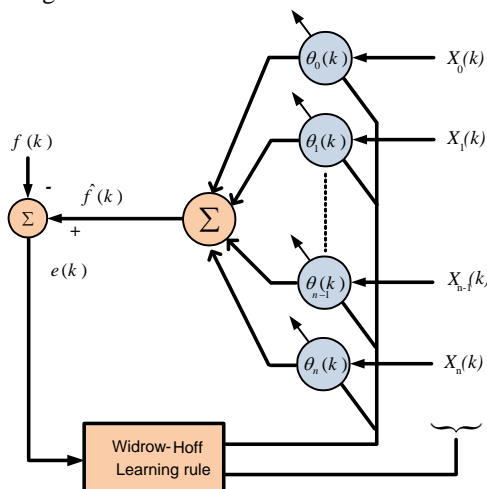


Figure 14. Structure of ADALINE.

Moreover, an ADALINE can be implemented to perform an on-line tracking of a given signal. Assume a given signal containing a harmonic component as follows:

$$f(t) = A_{dc}e^{-\beta t} + \sum_{i=1}^N F_i \sin(i\omega t(k) + \varphi_i) \tag{4}$$

where $A_{dc}e^{-\beta t}$ is transient DC component and β is damping time constant, φ_i is the phase and F_i is the magnitude of the i th harmonic. N indicates the total number of harmonics and ω signifies the main frequency and is assumed to be constant. If $f(t)$ is transferred to discrete time domain we have:

$$f(k) = a_{dc}(1 - \beta kT_s) + \sum_{i=1}^N \{a_i \sin(i\omega t(k)) + b_i \cos(i\omega t(k))\} \tag{5}$$

Where $a_{dc}(1 - \beta kT_s)$ are the first two terms of Taylor expansion of the transient DC component, $T_s = 2\pi / \omega N_s$ and N_s indicates the sampling period. Also, $a_i = F_i \cos \varphi_i$, $b_i = F_i \sin \varphi_i$ and $t(k)$ is the k th sampling time. $X(k)$ signifies the input vector:

$$X(k) = [\sin \omega t(k) \cos \omega t(k) \dots \sin n\omega t(k) \cos n\omega t(k) 1 - kT_s]^T \tag{6}$$

Where $\theta(k)$ is the weight vector of ADALINE. Therefore, the inner product of $\theta(k)$ with $X(k)$ is equal to the ADALINE output:

$$f(k) = \sum_{i=1}^N \theta_i(k) X_i(k) = \theta(k) X^T(k) \tag{7}$$

The weight vector $\theta(k)$ is addressed by discrete Fourier transform coefficients of $f(k)$ during the learning process. In order to minimize the error between ADALINE output and target signal, the weights should be chosen appropriately in the learning phase. For training the ADALINE, Widrow-Hoff learning rules based on the least square error approach are utilized [32]. Also, the weights are corrected as follows:

$$\theta(k+1) = \theta(k) + \eta \frac{e(k)X(k)}{X^T(k)X(k)} \tag{8}$$

Where $\theta(k)$ and $\theta(k+1)$ are the weight vectors at k th and $(k+1)$ th sample respectively. $X(k)$ refers to the input vector at k th sample and the error function is $e(k) = \hat{f}(k) - f(k)$. Also η signifies the learning rate.

In order to have a precise tracking of $f(k)$, the error function should be smaller than a threshold value. If this condition is satisfied, $f(k)$ is written as:

$$f(k) = \hat{f}(k) = \theta_o X^T(k) \tag{9}$$

where $\hat{f}(k)$ is the target signal. Also, the weight vector θ_o in (9) is defined by (10):

$$\theta_o = [a_1 \ b_1 \ \dots \ a_N \ b_N \ a_{dc} \ \beta a_{dc}] \tag{10}$$

After obtaining the weights vector, the harmonic content of the under study waveform at k th sample is calculated by equations (11) and (12):

$$F_n(k) = \sqrt{\theta_{2n-1}^2(k) + \theta_{2n}^2(k)} \tag{11}$$

$$\varphi_n(k) = \cos^{-1} \left(\frac{\theta_{2n}(k)}{F_n(k)} \right) \ , \ (n = 1, 2, \dots, N) \tag{12}$$

6.1. ADALINE Training Algorithm

Training algorithm is the main characteristic of the Artificial Neural Network (ANN), and the training process of ADALINE is also the process of modifying the weights of the network [33]. Through this, the error between the desired output, $\tilde{z}(k)$, and the actual output, $z(k)$, can be minimized. Widrow-Hoff learning rules are adopted here. Firstly, an output error function of the linear network is defined as:

$$E = \frac{1}{2} \sum_k [\tilde{z}(k) - z(k)]^2 = \frac{1}{2} \sum_k [\tilde{z}(k) - \theta(k)X^T(k)]^2 \quad (13)$$

Because E is dependent on the weights and the desired output, we can regulate the weights to minimize E . Widrow-Hoff learning rules are based on an approximate steepest descent procedure. Widrow and Hoff had the insight that they could estimate the mean square error by using the squared error for each iteration. If we take the partial derivative of the squared error with respect to the weights and biases at the k th iteration, we have:

$$\begin{aligned} \Delta\theta_i(k) &= -\alpha \frac{\partial E}{\partial \theta_i(k)} = -\alpha [\tilde{z}(k) - \theta(k)X^T(k)]X_i(k) \\ &= \alpha e(k)X_i(k) \end{aligned} \quad (14)$$

where α is the learning rate, generally $\alpha \in (0,1)$. If α is large, learning occurs quickly, but if it is too large, it may lead to instability and errors may even increase. To ensure a stable learning, the learning rate must be less than the reciprocal of the largest eigen value of the correlation matrix $X^T(k)X(k)$ of the input vectors. Thus, weight increase is

$$\Delta\theta(k) = \alpha \frac{e(k)X(k)}{\lambda + X^T(k)X(k)} \quad (15)$$

where $\alpha \in (0,1)$. To produce a faster convergence in the presence of random noise, a non-linear weight adaptation algorithm is desirable. Therefore, the weight adjustment algorithm is written as:

$$\Delta\theta(k) = \alpha \frac{e(k)X(k)}{\lambda + X^T(k)\phi(k)} \quad (16)$$

where

$$\phi(k) = \begin{bmatrix} SGN(x_1) \\ SGN(x_2) \\ \vdots \\ SGN(x_n) \end{bmatrix}, \quad (17)$$

with

$$SGN(x) = \begin{cases} +1 & \text{if } x \geq 0 \\ -1 & \text{if } x < 0 \end{cases} \quad (18)$$

Widrow-Hoff learning rules state that the change of the net weights has a direct proportion to the output error and the inputs of the ADALINE. This algorithm does not need to calculate the derivatives. Hence, it can be computed simply and makes the ADALINE converge fast. From Fig. 3 and Eq. (12), each iteration needs only $2N$ multiplications and $N+5$ additions (N is the number of inputs). Therefore, it can be easily implemented through hardware and is good for on-line

usage.

The training process of ADALINE includes three steps:

I) Calculate the network output $z(k) = \theta(k)X^T(k)$ and the error $e(k) = \tilde{z}(k) - z(k)$.

II) Compare the network output sum of square errors, E , and the target error, E_0 . If E is smaller than E_0 or the training iterations already reached the maximum limit, stop training; otherwise continue.

III) Calculate new weights, $\theta(k+1) = \theta(k) + \Delta\theta(k)$, and return to step I).

This neural network is used in this study to extract the residual current waveform harmonics. Since the ADALINE neural network is very quick and simple in calculations and implementation, it can be used instead of the Fourier analysis method. According to the results in [32], the convergence time in ADALINE-based method is less than half a cycle, while it takes a minimum of one complete cycle for the Fourier analysis to estimate the harmonics.

One sample of the residual current affected by a HIF has been simulated on the test network explained in Section 4. In addition, the residual current waveform at the beginning of the line has been given in Fig. 15 along with the signal waveform (which tracks the main signal in order to extract its harmonic content) trained by the ADALINE. This figure indicates that the neural network has performed the tracking activity very precisely and quickly.

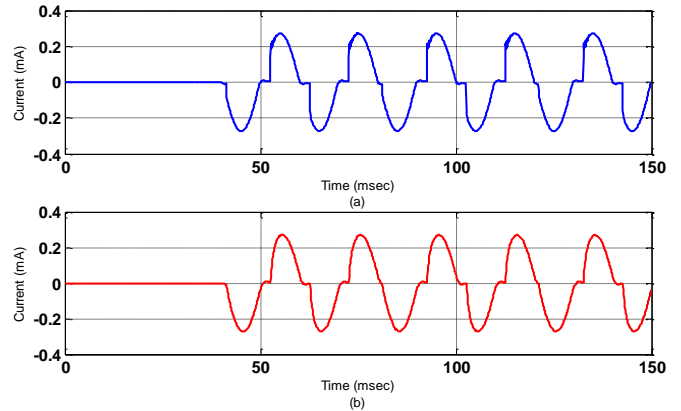


Figure 15. a) The residual current waveform at the beginning of line b) The trained signal.

7. HIF DETECTION ALGORITHM

The harmonic index used in this paper comprises both even and odd harmonics simultaneously. Equation (19) demonstrates the proposed index called FDI (Fault Detection Index) at the k th sample:

$$\begin{aligned} FDI(k) &= \frac{\sum_{i=1}^3 H_{2i-1}(k)}{\sum_{i=1}^3 H_{2i}(k)} \\ &= \frac{\sum_{i=1}^3 \sqrt{\theta_{(4i-3)}^2(k) + \theta_{(4i-2)}^2(2k-1)}}{\sum_{i=1}^3 \sqrt{\theta_{(4i-1)}^2(k) + \theta_{(4i)}^2(2k-1)}} \end{aligned} \quad (19)$$

Where $H_{2i-1}(k)$ and $H_{2i}(k)$ are odd and even harmonics at the

k th sample respectively and θ indicates ADALINE weighting coefficients after the convergence. The threshold value of 1 is selected after applying HIFs on different points of the test network and running different simulations. Fig. 16 shows the residual current waveform along with the FDI for the HIF discussed in Section 5. Upon the fault happens, the value of FDI exceeds the selected threshold and this is the indicator of a HIF occurrence.

The function of the proposed algorithm for HIF detection has been shown in the flowchart of Fig. 17.

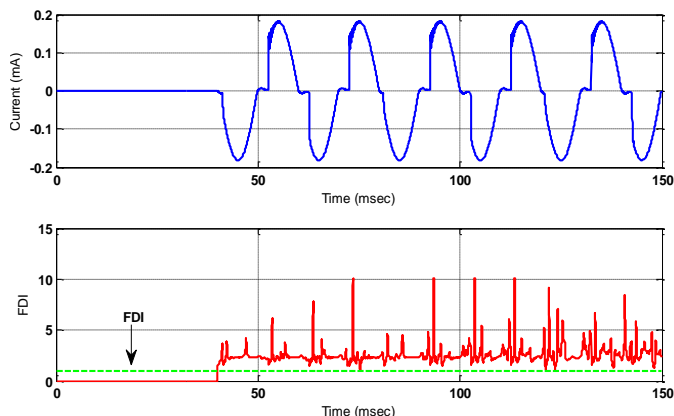


Figure 16. The residual current waveform with FDI for the HIF discussed in Section 5.

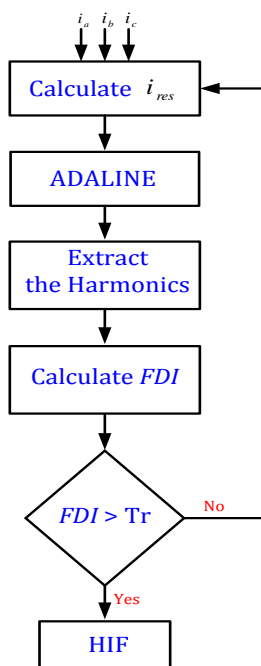


Figure 17. Flowchart of the proposed algorithm for HIF diagnosis.

8. SIMULATION RESULTS AND DISCUSSION

In order to analyze the proposed approach in the presence of similar occurrences in the power distribution network, different experiments listed below have been applied:

- a) Inserting the capacitor bank into the network
- b) Removing the capacitor bank from the network
- c) Applying overloads to the network

- d) Full load trans switching
- e) Injecting the solar power into the network
- f) Injecting the wind power into the network
- g) Removing the wind power from the network
- h) HIF occurrence

If the HIF can be recognized from other similar situations truly, it can be inferred that the proposed approach is a very efficient solution which can be used in power distribution networks containing renewable resources. In all above situations, a HIF is embedded in 4 km line L1 and measuring devices are placed at the beginning of line L1. Figure 18 shows FDI with the residual current waveforms for all the eight situations. It is obvious that only in HIF situation the FDI exceeds the threshold value and this verifies that the proposed approach has recognized the HIF truly.

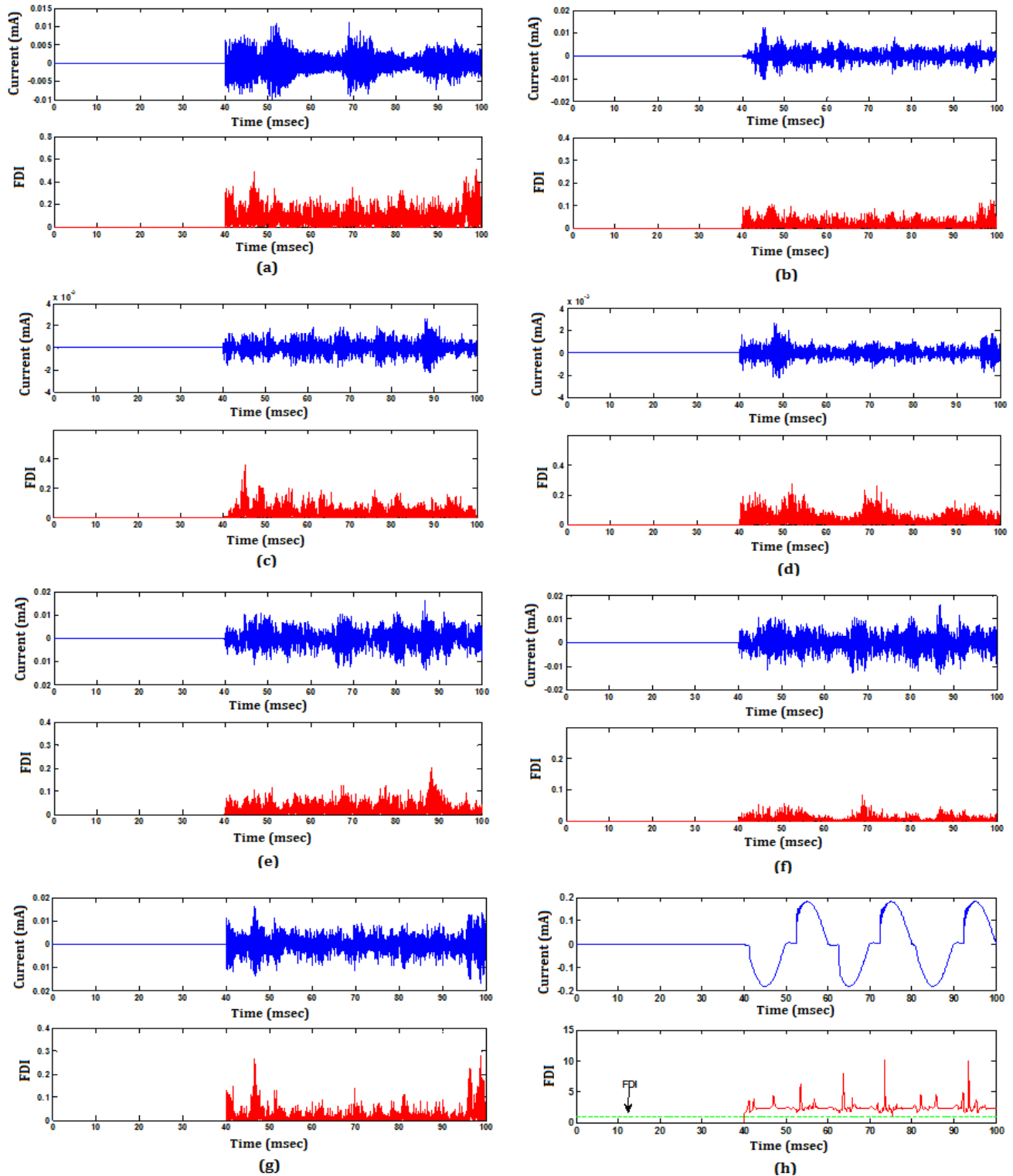
Through the other experiment, various HIFs with different resistances were applied in different points of lines L1 and L3 while the measuring devices were placed at the beginning of the line. The proposed approach performed this test correctly too and was able to recognize the HIF occurrence. The figures of this test have not been presented for the sake of conciseness.

9. CONCLUSION

In this paper the most common methods for HIF modeling were studied firstly. Then a complete arcing model was introduced which models the exact behavior of HIF in the positive and negative half-cycles. Afterwards, an ADALINE-based algorithm for accurate detection of HIFs in power distribution networks was proposed. In the proposed approach, the residual current at the beginning of the line is calculated firstly and then this new extracted waveform is given to ADALINE. The harmonics of the residual current waveform are calculated through the quick accurate tracking conducted by ADALINE. In the next step, HIFs are recognized from other similar situations such as capacitor switching or overloading via a harmonic criterion. The test network of this study was included with renewable energy resources like the solar and wind resources. As the simulation results confirm, quickness and high precision, independence from fault location, independence from fault location impedance, and the accurate diagnosis in the presence of new distribution networks with DG resources are the most valuable characteristics of the proposed approach.

REFERENCES

- [1] Aucoin M. A, Russel B. D, and Benner C. L, "High impedance fault detection for industrial power systems," *Industry Applications Society Annual Meeting, Conference Record of the 1989 IEEE*, 2: 1788–1792 (1989).
- [2] Silva P. R, Santos A. Jr, and Jota F. G, "An intelligent system for automatic detection of high impedance fault in electrical distribution systems," *Circuits and Systems, Proceeding of the 38th Midwest Symposium on*, 1: 453-456 (1996).
- [3] Santos W. C, Costa F. B, Silva J. A. C. B, Lira G. R. S, Souza B. A, Brito N. S. D, and Paes Junior M. R. C, "Automatic building of a simulated high impedance fault database," *PES Transmission and Distribution Conference and Exposition: Latin America, IEEE*, 550-554 (2010).



**FDI with the residual current waveforms for situations: a) Inserting the capacitor bank into the network
b) Removing the capacitor bank from the network c) Applying overloads to the network
d) Full load trans switching e) Injecting the solar power into the network
f) Injecting the wind power into the network g) Removing the wind power from the network
h) HIF occurrence**

- [4] Ramazani M. J, Gandomkar M, and Nayebi V, "High impedance fault detection techniques over the time" 15th Iranian Student Conference on Electrical Engineering, (in Persian), (2012).
- [5] Geerings D. L, and Linders J. R, "A practical protective relay for down conductor faults," *IEEE Transactions on Power Delivery*, 6(2): 565-574 (1991).
- [6] Russell B. D, Mehta K, and Chinchali R. P, "An arcing fault detection technique using low frequency current components performance evaluation using recorders field data," *IEEE Transactions on Power Delivery*, 3(4): 1493-1500 (1988).
- [7] Kwon W. H, Park Y. M, Yoon M. C, and Yoo M. H, "High impedance fault detection utilizing incremental variance of normalized even order harmonics power," *IEEE Transactions on Power Delivery*, 6(2): 557-564 (1991).
- [8] Shahrtash M, and Jadid Sh, "Detection of high impedance faults with arc happening in power systems" *MSc Thesis, Iran University of Science and Technology*, (in Persian) (1999).
- [9] Thakallapelli A, "Detection of high impedance faults by distance relays using prony method," *International Journal of Advanced Technology & Engineering Research*, 2(2): 39-45 (2012).
- [10] Hanninen S, Lehtonen M, "Method for detection and location of very high resistive earth faults," *European Transactions on Electrical Power*, 9(5): 285-291 (1999).
- [11] Samantaray S. R, "Ensemble decision trees for high impedance fault detection in power distribution network," *International Journal of Electrical Power and Energy Systems, Elsevier Science*, 43(1): 1048-1055 (2012).
- [12] Singh A. K, and Parida S. K, "A multiple strategic evaluation for fault detection in electrical power system," *International Journal of Electrical Power and Energy Systems, Elsevier*, 48: 21-30 (2013).
- [13] Samantaray S, Tripathy L, and Dash P, "Combined EKF and SVM based high impedance fault detection in power distribution feeders," *International Conference on Power Systems (ICPS '09), IEEE*, 1-6 (2009).
- [14] Nikofar I, Sarlak M, and Shahrtash M, "High impedance fault detection in distribution networks using TT transform and vector support machine" *4th Power Systems Protection & Control Conferenc, (in Persian)* (2009).
- [15] Keyhani R, Deriche M, and Palmer E, "A high impedance fault detector using a neural network and sub-band decomposition," *IEEE Conference on Signal Processing and its Applications*, 458-461 (2001).
- [16] Huang S. J, and Wan H. H, "Feature extraction-enhanced wavelet transform computation for high impedance fault detection," *International Journal of Computer, Consumer and Control (IJ3C)*, 2(1): 18-25 (2013).
- [17] Torres V, and Ruiz H. F, "High impedance fault detection using discrete wavelet transform," *IEEE Conference on Electronics, Robotics and Automotive Mechanics*, 325-329 (2011).
- [18] Etemadi A. H, and Sanaye-Pasand M, "High impedance fault detection using multi-resolution signal decomposition and adaptive neural fuzzy inference system," *IET Journal of Generation, Transmission & Distribution*, 2(1): 110-118 (2008).
- [19] Gautam S, and Brahma S. M, "Detection of high impedance fault in power distribution systems using mathematical morphology," *IEEE Transactions on Power Systems*, 28(2): 1226-1234 (2013).
- [20] Aucoin M, Status of high impedance fault detection, *IEEE T-PAS-104*, (3): 638-643 (1985).
- [21] Emanuel A. E, Cyganski D, Orr J. A, Shiller S, Gulachenski E. M, "High impedance fault arcing on sandy soil in 15 kV distribution feeders: contributions to the evaluation of the low frequency spectrum", *Power Delivery, IEEE Transactions on*, 5(2): 676-686 (1990).
- [22] Sharaf A. M, Snider L. A, Debnath K, "A neural network based error propagation relay algorithm for distribution system high impedance fault detection", *Advances in Power System Control, Operation and Management, 2nd International Conference on*, 613-620 (1993).
- [23] Chan D, Wai T, Yibin X, "A novel technique for high impedance fault identification", *Power Delivery, IEEE Transactions on*, 13(3): 738-744 (1998).
- [24] Nam S. R, Park J. K, Kang Y. C, Kim T. H, "A modeling method of a high impedance fault in a distribution system using two series time-varying resistances in EMTP", *Power Engineering Society Summer Meeting, IEEE*, 1175-1180 (2001).
- [25] Lai T. M, Snider L. A, Lo E, "Wavelet Transform Based Relay Algorithm for the Detection of Stochastic High Impedance Faults", *International Conference on Power System Transient, in New Orland, IPTS*, 1-6 (2003).
- [26] Sheng Y, and Rovnyak S. M, "Decision Tree-Based Methodology for High Impedance Fault Detection", *Power Delivery, IEEE Transactions on*, 19(2): 533-536 (2004).
- [27] Michalik M, Rebizant W, Lukowicz M, Lee S.-J, Kang, "Wavelet Transform Approach to High Impedance Fault Detection in MV Networks", *Proceedings of the 2005 IEEE PowerTech Conference*, June 2005.
- [28] Michalik M; et al, "High-Impedance Fault Detction in Distribution Networks With Use of Wavelet-Based algorithm", *IEEE Transactions on Power Delivery*, 21(4): 1793-1802 (2006).
- [29] Elkalashy N, Lehtonen M, Darwish H, Izzularab M, and Taalab A, "Modeling and experimental verification of a high impedance arcing fault in MV networks". *IEEE Transactions on Dielectric and Electrical Insulation*, 14(2): 375-383 (2007).
- [30] Eslami L, and Keivanian R, "Precise Modeling and Detection of High Impedance Faults in Microgrid System Based on Residual Current Harmonic Analysis" *International Review of Electrical Engineering (IREE)*, 7(1): 3523-3531 (2012).
- [31] Zhang, W.: 'A Generalized ADALINE Neural Network for System Identification', *International Conference on Control and Automation, IEEE*, 2007; p. 2705 - 2709
- [32] Vahidi, B., Jannati, M., and S. H. Hosseinian.: 'A Novel Approach to Adaptive Single Phase Autoreclosure Scheme for EHV Power Transmission Lines Based on Learning Error Function of ADALINE', *T. SOC. MODEL. SIMUL.*, 2008, 84, (12), p. 601-610
- [33] Wang, Z. Q., Manry, M. T., and Schiano, J. L.: 'LMS learning algorithms: misconceptions and new results on convergence' *IEEE. T. Neural. Networ.*, 2000, 11, (1), p. 47-56